Heat Transfer Enhancement of Cylindrical Heat Pipes Using Lattice Boltzmann Method

Kods Grissa, Zied Lataoui, and Abdelmajid Jemni
Laboratory of Thermal and Energetic Systems Studies (LESTE) at the National School of Engineering of Monastir, University of Monastir, Tunisia
Email: kods.grissa@ensma.fr

Kods Grissa, Adel Benselama, and Yves Bertin
Institut Pprime, CNRS - ENSMA - Université de Poitiers, Département Fluides, France

***Abstract*—A pseudo three dimensional numerical analysis is presented for simulation of cylindrical heat pipe using the Lattice Boltzmann method. The analysis includes the heat conduction in the wall and liquid-wick regions as well as the vapor region. Comparisons between the present model and previous numerical results showed very good agreement. The estimations of the liquid and vapor velocity profiles and temperature distributions are also presented and discussed. It is shown that the vapor flow field remains nearly symmetrical about the heat pipe centerline. Numerical results under different working conditions are presented, which provide guidance for the heat pipe design.**

***Index Terms*—heat pipe, heat flux, lattice Boltzmann method, heat transfer**

I. Introduction

Over the last several decades, the advancing technology of devices requires a higher level of heat rejection efficiency in order to overcome its thermal management constraints and challenges. As reliable and efficient passive heat recovery devices, Heat Pipe (HP) is a promising candidate to meet those constraints for many years with the development of new types such as loop heat pipes, micro and miniature heat pipes, and pulsating Heat Pipes (HPs) [1]. It provides high transfer rates over large distances, with minimal temperature drops, excellent flexibility, simple construction, less maintenance and easy control, all without a need for external pumping power.

Due to its several advantages, HPs are currently used as standard tools in a wide variety of heat transfer related applications such as electronics cooling [1], heat exchangers [2], heat recovery in renewable energy [3], space applications [4] and so on. As a result of the strong interest in HP technology and its applications, several analytical [5], experimental [6] and numerical [7] analyses have been carried out by many investigators to facilitate the understanding of HP operation with a significantly progress. For the simplicity of presentation, only the very recent works are reviewed here. By highlighting the contribution of HP in reducing the carbon emissions to the environment, a detailed review of HP application ranging from computer electronics to renewable energy was presented by Mochizuki *et al*. [1]. Later, Faghri [8] reported the progress of HP from its invention to now days by describing its recent advancement in manufacturing, simulation and its applications. Chaudhry *et al*. [3] evaluated the current HP systems for heat recovery and renewable applications utility. Basic features and limitations are outlined and theoretical comparisons are drawn with respect to the operating temperature profiles for the reviewed industrial systems. More recently, Shabgard *et al*. [2] reviewed the different type, the opportunities and challenges related to current HP heat exchangers applications.

From the above literature, the Lattice Boltzmann Method (LBM) has not been used to predict the performance of a wicked heat pipe, although this method is used to deal with a complicated problem and provides efficient and accurate results [9], [10]. Deriving motivation from this, the present study aims to model the two dimensional heat transfers and fluid flow in a cylindrical HP using the LBM.

II. Problem Definition

The operation of a conventional HP involves the evaporation of a working fluid at the evaporator section. Due to the pressure difference, the resulting vapor migrates along the length of the central vapor core through the adiabatic section to the condenser section, where it condenses by releasing its latent heat of vaporization to the provided heat sink. Then, the condensed fluid flows back to the evaporator section end by the capillary pressure created by the menisci in the wick pumps. This process will continue as long as there is a sufficient heat input to the heated section. The physical configuration of a HP is illustrated in Fig. 1.

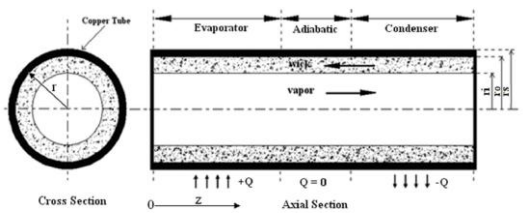

Figure 1. Schematic of conventional cylindrical heat pipe.

Manuscript received October 19, 2016; revised January 18, 2017.

doi: 10.18178/ijmerr.6.2.82-87

The analysis is carried out for an incompressible, laminar and two-dimensional axisymmetric flow without any external effects. The porous structure is saturated with a single phase Newtonian fluid and considered homogenous and isotropic with a uniform porosity and uniform permeability magnitude. Furthermore, the thermos-physical properties of the working fluid and solid matrix are supposed to be constant. The liquid and vapor phases are coupled at the liquid-vapor interface.

III. Governing Equations

A. The Governing Equations

Under the above assumptions, the final form of the governing equations based on the Representative Elementary Volume (REV) is given by Eqs. (1)–(4):

- *Continuity equation:*

$$\frac{\partial u_r}{\partial r}+\frac{u_r}{r}+\frac{\partial u_z}{\partial z}=0 \tag{1}$$

- *Momentum equation:*

$$\frac{\partial u_z}{\partial t}+\frac{1}{\varepsilon}\left(u_r\frac{\partial u_z}{\partial r}+u_z\frac{\partial u_z}{\partial z}\right)=-\frac{\varepsilon}{\rho}\frac{\partial p}{\partial z}+\nu_e\left[\frac{\partial^2 u_z}{\partial r^2}+\frac{1}{r}\frac{\partial u_z}{\partial r}+\frac{\partial^2 u_z}{\partial z^2}\right]+F_{pz} \tag{2}$$

$$\frac{\partial u_r}{\partial t}+\frac{1}{\varepsilon}\left(u_r\frac{\partial u_r}{\partial r}+u_z\frac{\partial u_r}{\partial z}\right)=-\frac{\varepsilon}{\rho}\frac{\partial p}{\partial r}+\nu_e\left[\frac{\partial^2 u_r}{\partial r^2}+\frac{1}{r}\frac{\partial u_r}{\partial r}-\frac{u_r}{r^2}+\frac{\partial^2 u_r}{\partial z^2}\right]+F_{pr} \tag{3}$$

- *Energy equation:*

$$\sigma\frac{\partial T}{\partial t}+u_z\frac{\partial T}{\partial z}+u_r\frac{\partial T}{\partial r}=\alpha_e\left[\frac{\partial^2 T}{\partial r^2}+\frac{1}{r}\frac{\partial T}{\partial r}+\frac{\partial^2 T}{\partial z^2}\right] \tag{4}$$

where u_r, u_z, p and T are the volume averaged radial velocity, axial velocity, pressure and temperature of the fluid, respectively. ν_e is the effective kinetic viscosity, $\sigma=\left(\varepsilon\rho_f c_{pf}+(1-\varepsilon)\rho_s c_{ps}\right)/\left(\rho_f c_{pf}\right)$, α_e is the effective thermal diffusivity coefficient which is equal to:

$$\alpha_e=\begin{cases}\dfrac{\lambda_e}{\varepsilon\rho_l C_{pl}}, \text{in the porous region}\\ \dfrac{\lambda_v}{\rho_v C_{pv}}, \text{in the vapor region}\end{cases} \tag{5}$$

where λ_e is the effective thermal conductivity:

$$\lambda_e=\frac{\lambda_l\left[(\lambda_l+\lambda_s)-(1-\varepsilon)(\lambda_l-\lambda_s)\right]}{\left[(\lambda_l+\lambda_s)+(1-\varepsilon)(\lambda_l+\lambda_s)\right]} \tag{6}$$

$\mathrm{F_p}=\left(F_{pz},F_{pr}\right)$ in (2) and (3) represents the total body force due to the presence of porous media which is given by:

$$\mathrm{F_p}=\left(F_{pz},F_{pr}\right)=\frac{\varepsilon\nu}{K}u_\phi-\frac{\varepsilon F_\varepsilon}{K}|u|u_\phi+\varepsilon G;(\phi=z,r) \tag{7}$$

where ε is the porosity of the porous medium; ν is the fluid viscosity which is not necessarily the same as the effective viscosity ν_e; $|u|=\sqrt{u_r^2+u_z^2}$ and **G** is the body force induced by an external force. The F_ε geometric function and the porous medium permeability K are related to the porosity based on Ergun's experimental investigations [11], as:

$$F_\varepsilon=\frac{1,75}{\sqrt{150}\varepsilon^{3/2}} \tag{8}$$

$$K=\frac{\varepsilon^3 d_p^2}{150(1-\varepsilon)^2} \tag{9}$$

where d_p is the diameter of the solid particle.

In the vapor region, the porosity ε gets very close to 1 with infinite permeability. Thus, the generalized momentum reduces to the Navier-Stokes equation.

For the wall region, the heat transfer is transferred purely by conduction as follows:

$$\frac{\partial T_s}{\partial t}=\alpha_s\left[\frac{\partial^2 T_s}{\partial r^2}+\frac{1}{r}\frac{\partial T_s}{\partial r}+\frac{\partial^2 T_s}{\partial z^2}\right] \tag{10}$$

where subscripts "s" refers to solid wall.

B. Boundary Conditions

- In the vapor region:

- $r=0, 0\le z\le L, \dfrac{\partial u_{z,v}(z,0)}{\partial r}=u_{r,v}(z,0)=0, \dfrac{\partial T_v(z,0)}{\partial r}=0$
- $r=r_i, 0\le z\le L, u_{z,v}(z,r_i)=0, u_{r,v}(z,r_i)=u_{r,i}(z,r_i), T_v(z,r_i)=T_{sat}(P_i)$
- $z=0, 0\le r\le r_i, u_{z,v}(0,r)=u_{r,v}(0,r)=0, \dfrac{\partial T_v(0,r)}{\partial z}=0$
- $z=L, 0\le r\le r_i, u_{z,v}(L,r)=u_{r,v}(L,r)=0, \dfrac{\partial T_v(L,r)}{\partial z}=0$

At the vapor–wick interface, the temperature is assumed to be the saturation temperature corresponding to the interface pressure. By applying Clausius–Clapeyron equation, the saturation temperature can be determined by:

$$T_{sat}=\left(\frac{1}{T_0}-\frac{R_v}{h_{fg}}\ln\frac{P_i}{P_0}\right) \tag{11}$$

where R_v is the gas constant for the vapor, T_0 and P_0 are the temperature and pressure reference, respectively.

By using the energy balance at the interface liquid–vapor, the boundary condition for the injection blowing and suction velocities v_i (z) which couples the vapor and the porous region of this interface is defined as:

$$Q+\lambda_e\frac{\partial T_l}{\partial r}=\rho_v h_{fg}u_{r,i} \tag{12}$$

In the porous region:

- $r=r_p, 0\le z\le L, u_{z,l}(z,r_p)=u_{r,l}(z,r_p)=0, \lambda_e\dfrac{\partial T_l(z,r_p)}{\partial r}=\lambda_s\dfrac{\partial T_s(z,r_p)}{\partial r}$
- $r=r_i, 0\le z\le L, u_{z,l}(z,r_i)=0, u_{r,l}(z,r_i)=u_{r,i}(z,r_i), T_l(z,r_i)=T_{sat}(P_i)$
- $z=0, 0\le r\le r_i, u_{z,v}(0,r)=u_{r,v}(0,r)=0, \dfrac{\partial T_v(0,r)}{\partial z}=0$
- $z=L, 0\le r\le r_i, u_{z,v}(L,r)=u_{r,v}(L,r)=0, \dfrac{\partial T_v(L,r)}{\partial z}=0$

In the wall region:

- $z=0, r_p\le r\le r_0, \dfrac{\partial T_s(0,r)}{\partial z}=0$
- $z=L, r_p\le r\le r_0, \dfrac{\partial T_s(L,r)}{\partial z}=0$

$$\bullet\, r = r_0, \begin{cases} -\lambda_s \dfrac{\partial T_s(z,r_s)}{\partial r} = -Q,\ 0 \le z \le L_e \\ -\lambda_s \dfrac{\partial T_s(z,r_0)}{\partial r} = 0,\ L_e \le z \le L_a \\ -\lambda_s \dfrac{\partial T_s(z,r_0)}{\partial r} = Q,\ L_e \le z \le L \end{cases}$$

$$\bullet\, r = r_p, 0 \le z \le L,\ \lambda_e \frac{\partial T_f(z,r_p)}{\partial r} = \lambda_s \frac{\partial T_s(z,r_p)}{\partial r}$$

C. Dimensionless form of the Governing Equations

By introducing the following dimensionless parameters:

$$R = \frac{r}{r_i}, Z = \frac{z}{r_i}, U_r = \frac{u_r}{u_i}, U_z = \frac{u_z}{u_i}, \theta = \frac{T}{T_i}, P = \frac{p}{\rho u_i^2}, t^* = \frac{u_i}{r_0} t$$

The fluid flows governed by equation (1-4) have the following dimensionless form:

- *Continuity equation:*

$$\frac{\partial U_r}{\partial R} + \frac{U_r}{R} + \frac{\partial U_z}{\partial Z} = 0 \tag{13}$$

- *Momentum equation:*

$$\frac{\partial U_z}{\partial t^*} + \frac{1}{\varepsilon}\left(U_r \frac{\partial U_z}{\partial R} + U_z \frac{\partial U_z}{\partial Z}\right) = -\frac{\varepsilon}{\rho}\frac{\partial P}{\partial Z} + \frac{1}{\mathrm{Re}}\left[\frac{\partial^2 U_z}{\partial R^2} + \frac{1}{R}\frac{\partial U_z}{\partial R} + \frac{\partial^2 U_z}{\partial Z^2}\right] - \frac{\varepsilon}{\mathrm{Re}\,Da} U_z - \frac{\varepsilon F_\varepsilon}{\sqrt{Da}} |U| U_z + \varepsilon G \tag{14}$$

$$\frac{\partial U_r}{\partial t^*} + \frac{1}{\varepsilon}\left(U_r \frac{\partial U_r}{\partial R} + u_z \frac{\partial U_r}{\partial Z}\right) = -\frac{\varepsilon}{\rho}\frac{\partial P}{\partial R} + \frac{1}{\mathrm{Re}}\left[\frac{\partial^2 U_r}{\partial R^2} + \frac{1}{R}\frac{\partial U_r}{\partial R} - \frac{U_r}{R^2} + \frac{\partial^2 U_r}{\partial z^2}\right] - \frac{\varepsilon}{\mathrm{Re}\,Da} U_r - \frac{\varepsilon F_\varepsilon}{\sqrt{Da}} |U| U_r + \varepsilon G \tag{15}$$

- *Energy equation:*

$$\frac{\partial \theta}{\partial t^*} + U_z \frac{\partial \theta}{\partial Z} + U_r \frac{\partial \theta}{\partial R} = \frac{1}{\mathrm{Pr}\,\mathrm{Re}}\left[\frac{\partial^2 \theta}{\partial R^2} + \frac{1}{R}\frac{\partial \theta}{\partial R} + \frac{\partial^2 \theta}{\partial Z^2}\right] \tag{16}$$

where the non-dimensional parameters are: the Darcy number Da, the Prandtl number Pr and the Reynolds number Re, respectively, defined as:

$$\mathrm{Re} = \frac{u_i r_i}{\nu_v}, Da = \frac{K}{r_i^2}, \mathrm{Pr} = \frac{\nu}{\alpha} \tag{17}$$

IV. Numerical Method

The LBM has been proved to be an efficient numerical method for modeling the fluid flows in various fields [9, 10]. In this section, the LBGK model based on the REV approach for axisymmetric thermal flows through porous media will be introduced.

A. Axisymmetric Formulation of the Lbm for Incompressible Fluid Flows Though Porous Media

In this study, the LBM with Double Distribution Function (DDF LBM) approach is used in this work [10]. The model is based on the BGK collision operator, and is constructed with the idea of pseudo-Cartesian translation.

1) Lattice boltzmann for the velocity field

In order to simulate the axisymmetric flows through porous media, we propose the following LB model with source and force terms:

$$f_k(x + c_k\Delta t, t + \Delta t) - f_k(x,t) = \frac{\Delta t}{\tau_f}\left(f_k^{eq}(x,t) - f_k(x,t)\right) + w_k F_1 \Delta t + \frac{\Delta t}{6} c_{ki} F_{2i} + \mathrm{F_k}\Delta t \tag{18}$$

where $f_k(x,t)$ is the density distribution function (DF) of particles; $f_k^{eq}(x,t)$ is the local equilibrium distribution function (EDF) of particles; Δt is the time step; x is the space vector, i.e, x=(z, r), c= $\Delta x / \Delta t$; c_{ki} is the component of c_k which is the velocity vector of a particle in the k link; w_k is the weight, F_1 is the source term defined as:

$$F_1 = -\frac{\rho u_r}{r} \tag{19}$$

F_{2i} is the force term given by:

$$F_{2i} = -\frac{\rho u_i u_r}{\varepsilon r} - \frac{2\rho\nu u_i}{r^2}\delta_{ir} \tag{20}$$

The last term on the right-hand side of equation (18), is accounted for by the total force due to the presence of the porous medium and other external force fields and is given by [10]:

$$F_k = \omega_k \rho\left(1 - \frac{1}{2\tau}\right)\left(\frac{c_k . F}{c_s^2} + \frac{uF : \left(c_k c_k - c_s^2 I\right)}{\varepsilon c_s^4}\right) \tag{21}$$

and τ_f is an effective relaxation time related to the single relation time τ as:

$$\tau_f = \begin{cases} \dfrac{1}{\tau}, r = 0 \\ \dfrac{1}{\tau}\left(1 + \dfrac{(2\tau - 1)c_{ki}\Delta t}{2r}\right), r \ne 0 \end{cases} \tag{22}$$

To include the effect of the porous medium, the equilibrium distribution function (EDF) of the D_nQ_b models is defined as follows [10]:

$$f_k^{eq} = w_k \rho\left[1 + \frac{c.u}{c_s^2} + \frac{uu : \left(c_k c_k - c_s^2 I\right)}{2\varepsilon c_s^4}\right] \tag{23}$$

We used the nine-velocity square lattice (D2Q9), where w_k is defined as:

$$w_k = \begin{cases} \dfrac{4}{9}, \alpha = 0 \\ \dfrac{1}{9}, \alpha = 1,3,5,7 \\ \dfrac{1}{36}, \alpha = 2,4,6,8 \end{cases} \tag{24}$$

and c_k is as follows:

$$c_k = \begin{cases} (0,0), \alpha = 0 \\ \lambda_k c\left[\cos\left(\dfrac{(k-1)\pi}{4}\right), \sin\left(\dfrac{(k-1)\pi}{4}\right)\right], \alpha \ne 0 \end{cases} \tag{25}$$

with λ_k is defined as:

$$\lambda_k = \begin{cases} 1, \alpha = 1,3,5,7 \\ \sqrt{2}, \alpha = 2,4,6,8 \end{cases} \tag{26}$$

Accordingly, the fluid density ρ and fluid velocity **u** can be defined by:

$$\rho = \sum f_k \tag{27}$$

$$\rho u = \sum f_k c_k + \frac{dt}{2}\rho F \tag{28}$$

It is noted that the force term **F** of Equation (5) also contains the velocity **u**. However, the velocity **u** could be obtained explicitly due to its quadratic nature of the equation (28) itself as:

$$u = \frac{v}{c_0 + \sqrt{c_0^2 + c_1|v|}} \tag{29}$$

where v is an auxiliary velocity defined as:

$$\rho v = \sum f_k c_k + \frac{dt}{2}\rho \varepsilon G \tag{30}$$

The two parameters in (29) can be obtained by:

$$c_0 = \frac{1}{2}\left(1 + \varepsilon \frac{dt}{2}\frac{\nu}{K}\right) \tag{31}$$

$$c_1 = \varepsilon \frac{dt}{2}\frac{F_\varepsilon}{\sqrt{K}} \tag{32}$$

Through the Chapman-Enskog procedure, the effective viscosity is defined as:

$$\nu_e = c_s^2\left(\tau_f - 0.5\right)dt \tag{33}$$

2) Lattice boltzmann for the temperature field

The following LBE is used to describe the evolution of the temperature field:

$$g_k(x + c_k\Delta t, t + \Delta t) - g_k(x,t) = \frac{\Delta t}{\tau_g}\left(g_k^{eq}(x,t) - g_k(x,t)\right) + w_k S_1 \Delta t \tag{34}$$

where g_k is the temperature distribution function, τ_g is the dimensionless relaxation time which is related to the thermal diffusivity through the Chapman-Enskog expansion by:

$$\alpha_e = \sigma c_s^2\left(\tau_g - 0.5\right)dt \tag{35}$$

and g_k^{eq} is the equilibrium temperature distribution function which is defined as:

$$g_k^{eq} = w_k T\left[1 + \frac{(c_k.u)}{c_s^2}\right] \tag{36}$$

The last term in (34) represents the source term due to the axisymmetric configuration. This term can be easily solved by using Finite Difference method:

$$S = \frac{\alpha}{r}\frac{\partial T}{\partial r} \tag{37}$$

Through the TDF, the temperature T of the system is defined as:

$$T = \frac{\sum g_k}{\sigma} \tag{38}$$

where σ is the heat capacity ratio which reflects the influence of porous media on the temperature field.

V. Results and Discussion

The numerical simulations are performed for copper-water wicked heat pipes with its dimension and water as working fluid shown in Table I. The results in Fig. 2 are compared with the numerical results given by [12] where a heat load of 5000 W/m^2 was applied to the pipe wall along the evaporator. Good agreement is observed.

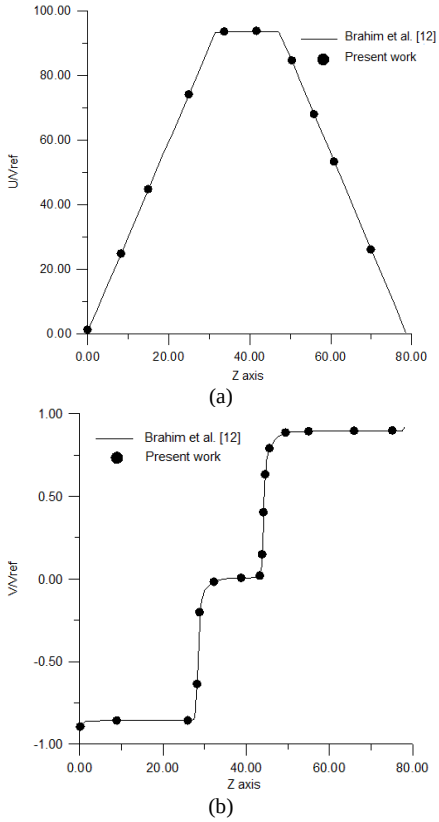

Figure 2. Vapor velocity profile: (a) axial velocity, (b) radial velocity

TABLE I. The Different Parameters of the Heat Pipe

Heat pipe wall	Wick structure	Vapor region
R=0.022 m L_{evap}=0.4 m L_{ad}=0.2 m L_{cond}=0.6 m L_{tot}=1.0 m λ_w=387.6 W/mK ρ_w=8978 kg/m^3 T_a=25 ℃ C_{pw}=381 J/kg K h_{conv}=800 W/m^2 K Material : copper	r_e=0.02 m ε=0.46 K=0.267*10^{-10} m^2 ρ_l=960.63 kg/m^3 λ_l=0.680 W/mK μ_l=2.8243 kg/ms C_{pl}=4216 J/kg K λeff=3.0476 W/mK Cpeff=3.8*106 J/kg K Material: sintered copper	r_e=0.0127 m ρ_v=0.599 kg/m^3 λ_v=0.0251 W/mK μ_v=0.129*10^{-4} kg/ms C_{pv}=1888 J/kg K h_{fg}=225.6267*10^4 J/Kg R_v=488 J/kg K T_{sat}=373.15 K

In the numerical calculations, the thermal properties of water are calculated at the reference temperature and they are assumed constant at this temperature except for the vapor density. A 5000 W/m^2 heat input was specified in the evaporator of the circumferentially-heated copper-water heat pipe model. Attention will first focus on the simulated heat pipe vapor flow.

Fig. 3 and Fig. 4 presents the distribution of velocity by varying different parameters. As it can be seen, the axial velocity along the pipe is divided into three equal parts. The location of the maximum axial velocity quickly migrates into the heat pipe centerline. The velocity distribution gradually approaches a parabolic profile towards the end of the heated region. The velocity distribution is practically symmetric about the heat pipe

centerline. This can be explained by the fact that the effective thermal conductivity of the wick is much smaller in comparison to the thermal conductivity of the heat pipe wall. Based on our numerical results, we conclude that the Reynolds number as well as the porosity affects the heat pipe operation. Indeed, as the Reynolds increases the velocity increases too. In the other hand, the augmentation of the porosity leads to the increase of the vapor velocity. This is can be explained by the fact that when the pores are too small the vapor diffuse more slowly which leads to the decrease in its velocity.

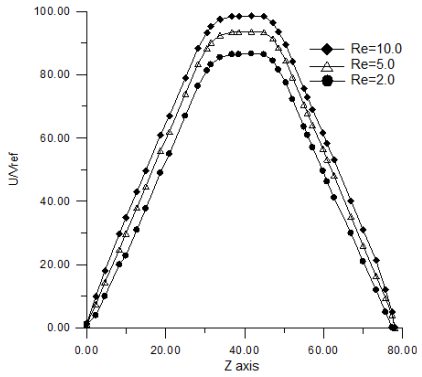

Figure 3. Radial vapor velocity for different reynolds number

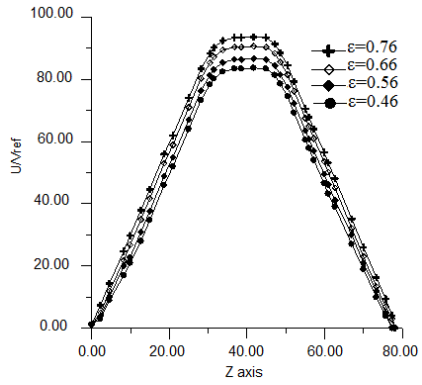

Figure 4. Radial vapor velocity for different porosity

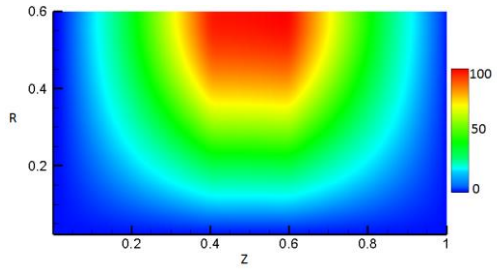

Figure 5. The axial vapor streamlines

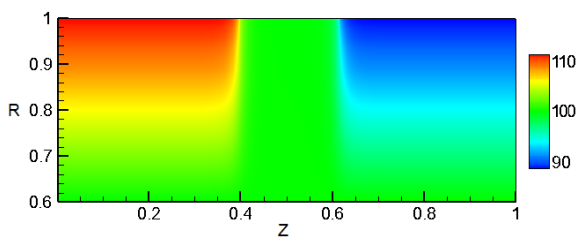

Figure 6. Liquid isotherms

The axial vapor streamlines velocity for the studied configurations are given in Fig. 5. As it can be seen, the axial vapor streamlines along the heat pipe are divided into three parts. At the evaporator region, the resulting vapor moves toward the condenser region via the adiabatic. One can see that the magnitude of the axial velocity increases as the evaporated working fluid mass is added to the vapor core from the evaporator end cap towards the adiabatic section.

Fig. 6 shows the temperature profile in the porous media for heat input condition of Q=5000W/m2. It can be observed that in the porous region, the heat transfer process occurs mainly by heat conduction. As it can be seen, three regions are observed: evaporator (heat in), adiabatic and condenser (heat out).

VI. Conclusion

A pseudo-three-dimensional numerical model has been developed for different part of cylindrical heat pipe, which includes vapor flow, liquid flow, and heat transfer in the porous wick structure and in the wall. The Lattice Boltzmann Method has been used for the first time to predict the performance of a wicked heat pipe. A new model was developed to solve the governing equations. The numerical results of the vapor were compared with the numerical data obtained previously which was in good agreement. The pertinence and the effects of various physical parameters were studied. It was found that the wall temperature distributions. Finally, a guideline and knowledge were obtained for designing a heat pipe.

References

[1] M. Mochizuki, T. Nguyen, K. Mashiko, Y. Saito, T. Nguyen, and V. Wuttijumnong, "A review of heat pipe application including new opportunities," *Frontiers in Heat Pipes*, vol. 2, no. 1, 2011.

[2] H. Shabgard, M. J. Allen, N. Sharifi, S. P. Benn, and A. Faghri, "Heat pipe heat exchangers and heat sinks: Opportunities, challenges, applications, analysis, and state of the art," *International Journal of Heat and Mass Transfer*, vol. 89, pp. 138-158, 2015.

[3] H. N. Chaudhry, B. R. Hughes, and S. A. Ghani, "A review of heat pipe systems for heat recovery and renewable energy applications," *Renewable and Sustainable Energy Reviews*, vol. 16, no. 4, pp. 2249-2259, 2012.

[4] V. V. Vlassov and R. R. Riehl, "Modeling of a loop heat pipe with evaporator of circumferential vapor grooves in primary wick," SAE Technical Paper, 2006.

[5] Y. Wang and K. Vafai, "Transient characterization of flat plate heat pipes during startup and shutdown operations," *International Journal of Heat and Mass Transfer*, vol. 43, no. 15, pp. 2641-2655, 2000.

[6] Y. Wang and K Vafai, "An experimental investigation of the transient characteristics on a flat-plate heat pipe during startup and shutdown operations," *Journal of Heat Transfer*, vol. 122, no. 3, pp. 525-535, 2000.

[7] R. Ranjan, J. Y. Murthy, and S. V. Garimella, "A numerical model for transport in flat heat pipes considering wick microstructure effects," *International Journal of Heat and Mass Transfer*, vol. 54, no. 1, pp. 153-168, 2011.

[8] A. Faghri, "Review and advances in heat pipe science and technology," *Journal of Heat Transfer*, vol. 134, no. 12, pp. 123001, 2012.

[9] Q. Li, K. Luo, Q. Kang, Y. He, Q. Chen, and Q. Liu, "Lattice Boltzmann methods for multiphase flow and phase-change heat transfer," *Progress in Energy and Combustion Science*, vol. 52, pp. 62-105, 2015.

[10] K. Grissa, R. Chaabane, Z. Lataoui, A. Benselama, Y. Bertin, and A. Jemni, "Lattice Boltzmann model for incompressible axisymmetric thermal flows through porous media," *Physical Review E*, vol. 94, no. 4, pp. 043306, 2016.
[11] S. Ergun, "Fluid flow through packed columns," *Chemical Engineering Progress*, vol. 48, pp. 89-94, 1952.
[12] T Brahim and A Jemni, "Effect of the heat pipe adiabatic region," *Journal of Heat Transfer*, vol. 136, no. 4, pp. 042901, 2014.

Kods Grissa graduated from the National Engineering School of Monastir (ENIM-Tunisia), in 2014 with a degree in Energy Engineering. Currently, she is a P.H. student in National Superior School of Mechanical and Aerotechnical (ENSMA- Poitiers) and National Engineering School of Monastir (ENIM- Monastir) working on the wicked heat pipe numerical modelisation and experimental study.

Yves Bertin Professeur at ENSMA and is doing his researches on Passive two-phase systems, thermal electric machines. Responsible for the COST research axis of the Institut P 'since 2010. The COST Research (Convection, Optimization and Thermal Systems) axis of the Institut P' brings together some thirty-people including 13EC and Researchers .

Abdelmajid Jemni Professeur at ENIM and is doing his researches on Passive two-phase systems, Hydrogen reactors. Responsible for the LESTE research laboratory. He is an editor in chef in many journals and participates to the comity chair of much congress.